On the Relation Between Geometrical Distance and Channel Statistics in In-Home PLC Networks

Fabio Versolatto and Andrea M. Tonello
WiPLi Lab - Università di Udine - Via delle Scienze 208 - 33100 Udine - Italy
e-mail: {fabio.versolatto, tonello}@uniud.it

***Abstract*—The concept of coverage in power line communications (PLC) is more difficult to be defined than in wireless systems. The main reason is that the PLC signal is conveyed by electrical wires and the wires follow an unpredictable path. We refer to the signal path length, and to the distance between the transmitter and receiver outlets as electrical distance and geometrical distance, respectively. The behaviour of the PLC channel is clearly a function of the electrical distance and it is reasonable to assume that the higher the geometrical distance, the higher the electrical distance.**

In this work, we focus on the PLC channel in in-home networks, and we discuss whether the statistics of the channel depends on the geometrical distance. We study the average channel gain, the root-mean-square delay spread, and the channel delay as a function of the geometrical distance. Furthermore, we address coverage, that we define in terms of maximum achievable rate as a function of the distance in the presence of additive colored Gaussian noise. We provide the linear relation between the metrics and the distance and the results are based on an experimental measurement campaign that we carried out in Italy, where we collected more than 1300 channel responses in multiple premises.

Finally, we propose a channel classification that is based on the geometrical distance.

I. Introduction

Power line communications (PLC) delivers data content by exploiting the existent power delivery infrastructure. We focus on the in-home scenario, where the existent standards ensure data rates of up to 200 Mbps by transmitting in the 2-30 MHz frequency band. New standards are coming out [1], [2]. They promise data rates of up to 1 Gbps, and they extend the signalling frequency range to 80 MHz.

The coverage is an open issue in PLC. In wireless, the coverage is associated to the geometrical distance between the transmitter and the receiver node. In PLC, the coverage depends on wirings. In-home wiring models have been presented in [3] and more recently in [4]. They are based on norms and common practices. Basically, the core node of the topology is the main panel. The main panel is the interconnection point between the in-home network and the energy supplier network. The main panel is connected to secondary nodes, namely, the distribution boxes, that feed the outlets. To minimize the wiring and to reduce the installation costs, nearby outlets are grouped and they are fed by the same derivation box. The connection between the outlets and the derivation box varies according to the practices and the norms of the different countries. In real-life topologies, the power line cables are buried in the walls and the path they follow from the derivation box to the outlets is typically not known. Thus, the length of the electrical connections cannot be measured with accuracy. Further, the appliances that are connected to the power delivery network impact on the propagation of the PLC signal.

The relation between the channel statistics and the topology can be investigated with the bottom-up approach. Bottom-up channel simulators were presented in [5] - [6], and random channel generators that are based on the bottom-up approach were described in [4], [7]. In [8], the bottom-up approach has been exploited to study the capacity as a function of the characteristics of the backbone. The backbone is the shortest signal path between the transmitter and the receiver outlet. It consists of connection cables, and interconnection nodes where the branches of the network depart from. The length of the backbone is the electrical distance between the transmitter and receiver outlets. Simulations show that the channel capacity seems to be not a function of the electrical distance [8]. Rather, it depends on the number of nodes of the backbone [8]. However, further experimental validations are required.

In this work, we follow a different approach. We address the relation between the distance and the statistics of the channel from experimental results (measurements).

To this aim, we performed an experimental measurement campaign in Italy. We collected channel frequency responses from different premises. The measurement sites are representative of small flats and detached houses that are located in the urban and suburban scenario. We followed a systematic approach. For each site, we identified the representative outlets and we measured the channel frequency response between all the couples of representative outlets. The channel frequency response is the ratio between the voltage at the receiver port, and the voltage at the transmitter port.

In [9], it has been shown that the channel frequency response is not symmetric. Therefore, given two outlets, we measured the channel frequency response on both directions. We collected more than 1300 channel acquisitions in the frequency domain. In this work, we focus on the 1.8-100 MHz frequency range, we gather the measured channels from different topologies all together, and we study the statistics of the resultant set. In detail, we study the average channel

The work of this paper has been partially supported by the FIT-IT-Project "Powerline Communications Systems in Nanometer CMOS Technology - xPLC, Project n. 830603".

gain (ACG), the root-mean-square (RMS) delay spread, and the maximum achievable rate as a function of the geometrical distance between the transmitter and the receiver. We compute the maximum achievable rate assuming the noise to be stationary, colored, additive and Gaussian. Furthermore, we address the channel delay, i.e., the delay that is introduced by the PLC channel.

Finally, we propose a novel channel classification. We group the channels into classes that are defined according to the geometrical distance between outlets. For each class, we provide the mean value of the main statistical metrics.

The remainder of this paper is divided as follows. In Section II, we describe the measurement campaign. We provide the details of the sites and the measurement setup. In Section III, we define the geometrical distance and we describe the statistical metrics that we consider. In Section IV, we provide the numerical results. Then, in Section V, we propose the channel classification and we provide the statistics of the channel classes. Finally, some conclusions follow.

II. Description of the Measurement Campaign

We performed a measurement campaign in Italy. In Italy, the energy supplier delivers the electricity by means of a three-phase distribution system, where four conductors are present, namely, three phases and the neutral. The neutral is the return wire and it is grounded at the transformer station.

Residential customers are connected to one phase and the neutral, i.e., a single-phase distribution system. In order to balance the load, different premises are alternatively connected to the three different phases. Conversely, industrial or commercial customers, that need more power, are connected to all three phases. Inside the premises, a third conductor is present. It is referred to as protective earth and it is deployed for safety reasons. The protective earth is grounded and, differently from US, it is not short-circuited to the neutral wire in the main panel.

The in-home power delivery network is split into different physical circuits, typically, two. They are connected to the energy supplier network through the circuit breakers that are placed in the main panel. The circuits are not supposed to feed distinct areas of the premise. Rather, they feed either major or small appliances, or either lights or loads. Therefore, they can be intended as high-power absorption and low-power absorption circuits.

The wires are enclosed into small plastic raceways and the Italian plugs are made of three in-line contacts. The central conductor is the protective earth, and thus the outlet and the plug are symmetrical w.r.t. the phase and the neutral. Recently, universal outlets have been also adopted and they allow for the connection of devices whose plug is compliant with the German and French standards.

We performed the measures in different sites. In Figure 1, we show the topology of one of the sites. Basically, they are representative of small urban flats and detached houses of the suburban scenario. The outlets are fed either by the same circuit breaker or by different circuit breakers. In the second case, the PLC channel may include the effect of the circuit breakers in the main panel. In the presence of multiple and adjacent outlets, we selected one of them as representative and we measured the channel frequency response between all the couples of representative outlets. We collected a total amount of 1312 channel responses. To our knowledge, this is one among the largest databases that has been reported in the literature.

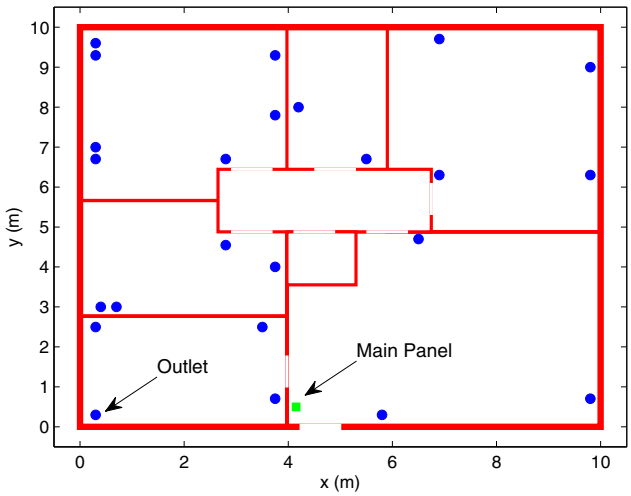

Fig. 1. Topology of one of the measurement sites.

A. Measurement Setup

We carried out the measurements in the frequency domain. Basically, we used a network analyzer (NA) in combination with two BNC-SMA extension cables, and two couplers. The extension cables allow for the measurements between distant outlets, and the couplers are high-pass filters that isolate the measurement equipment from the mains.

The NA allows for the measure of the scattering parameters (s-parameters) between two outlets of the network. In the following, we refer to the outlets as ports of the network.

We calibrated the NA when the extension cables were connected, and we removed the effect of the couplers as follows. Firstly, we characterized the couplers in terms of ABCD matrix. We note that the ABCD matrix representation can be directly obtained from the scattering parameters. Then, we exploited the chain rule of the ABCD matrices to remove the effect of the couplers from the measures. For further details on the ABCD matrices, please refer to [10]. The approach we followed has shown to be more reliable than calibrating the NA when the couplers were connected.

Now, the NA acquires a finite number of points, namely $N = 1601$. Thus, the frequency resolution Δf is equal to 62.5 kHz for measures in the frequency range up to 100 MHz. We denote with B_1 and B_2 the start and the stop frequency of the signalling bandwidth, respectively. In detail, $B_1 = 1.8125$ MHz and $B_2 = 100$ MHz.

Finally, to reduce the noise impairments, we averaged subsequent acquisitions of the channel. From measurements,

we have found that the average of 16 subsequent acquisitions is sufficient to cope with noise.

III. Channel Statistics and Distance

From the s-parameters, we extract the channel frequency response. We define the channel frequency response as the ratio between the phasors of the voltage at the receiver and the transmitter port. We use the frequency-discrete representation and the compact notation k to indicate the frequency $f = k\Delta f$, where $k = 0, \ldots, N-1$. In the following, $B_1 = N_1 \Delta f$. Furthermore, we denote the phasors of the voltage at the transmitter port and the receiver port as $V_{tx}(k)$ and $V_{rx}(k)$, respectively. Thus, the channel frequency response reads $H(k) = V_{rx}(k)/V_{tx}(k)$.

Given the transmitter and the receiver outlet, we model the power delivery network as a two-port network. Now, the s-parameter matrix of a two-port network is a 2×2 matrix with elements $s_{ij}(k)$, where $i, j = 1, 2$. If let the load impedance be equal to the characteristic impedance of the extension cables, 50 Ω in our case, and we assume the transmitter to be connected to port 1 and the receiver to be connected to port 2, we obtain

$$H(k) = \frac{V_{rx}(k)}{V_{tx}(k)} = \frac{s_{21}(k)}{1 + s_{11}(k)} \quad N_1 \leq k \leq N. \tag{1}$$

From the channel frequency response, we compute the real channel impulse response by means of inverse discrete Fourier transform (IDFT). Strictly, the real channel impulse response is the $2N-1$-points IDFT of the channel frequency response. We denote with $h(i)$ the real impulse response at the time instant $t = iT$, where $i = 0, \ldots, 2N-1$ and T is the resolution in time.

To reduce the side lobe effects, we cut the tails as follows. We compute the channel energy as

$$E = |H(0)|^2 + 2\Delta f \sum_{k=1}^{N-1} |H(k)|^2, \tag{2}$$

and we limit the channel impulse response to the one that includes 99 % of the channel energy.

In the following, we firstly define the geometrical distance between the outlets. Then, we describe the statistical metrics that we consider. From the channel frequency response, we compute the ACG, and the maximum achievable rate. From the channel impulse response, we compute the RMS delay spread, and the time of arrival.

A. Geometrical Distance

We compute the geometrical distance as follows. For each measurement site, we identify a reference point in the topology, say, a corner of the external walls. Then, from the reference point, we determine the three-dimensional coordinates of the outlets. We note that three dimensions are required because the sites may consist of multiple floors. The geometrical distance is the euclidean norm between the coordinates of the transmitter and the receiver outlet. In the following, we refer to the geometrical distance between the transmitter and the receiver outlet simply as distance, and we denote it with d.

B. Average Channel Gain

The ACG is a scalar metric that describes the frequency behaviour of the channel. We focus on the dB-version of the ACG, and we define it as follows

$$G = 10 \log_{10} \left(\frac{1}{N - N_1} \sum_{k=N_1}^{N-1} |H(k)|^2 \right) \quad [dB], \tag{3}$$

where we limit the ACG between B_1 and B_2. In the literature, it has been shown that the dB-version of the ACG is normally distributed [11]. In Section IV, from the experimental results, we confirm the normality of the ACG.

C. RMS Delay Spread

The RMS delay spread accounts for the energy spread of the channel impulse response. Basically, it is defined as follows

$$\sigma_\tau = T \sqrt{\frac{\sum_{i=0}^{2N-1} (i)^2 |h(i)|^2}{\sum_{i=0}^{2N-1} |h(i)|^2} - \left(\frac{\sum_{i=0}^{2N-1} i|h(i)|^2}{\sum_{i=0}^{2N-1} |h(i)|^2} \right)^2} \quad [s]. \tag{4}$$

In PLC, the RMS delay spread can be assumed to be distributed as a log-normal random variable [11]. This is also confirmed by our measurement results (see Section IV).

D. Achievable Rate

In this Section, we study the maximum achievable rate of the channel in the presence of stationary additive colored Gaussian noise. We assume transmission in 1.8-100 MHz, and the transmitted signal to be normally distributed. We denote with $P_{tx}(k)$, and $P_w(k)$ the PSD of the transmitted signal, and the noise, respectively. We assume the PSD of the transmitted signal to be equal to 10^{-5} mW/Hz up to 30 MHz, and to 10^{-8} mW/Hz above 30 MHz.

Concerning noise, we exploit the results that have been presented in the literature. Basically, we model the noise as additive colored Gaussian noise with PSD [12]

$$P_w(k) = \frac{1}{(k\Delta f)^2} + 10^{-15.5} \quad [mW/Hz]. \tag{5}$$

Finally, we compute the maximum achievable rate of the PLC channel as follows

$$R = \Delta f \sum_{k=N_1}^{N-1} \log_2 \left(1 + \frac{|H(k)|^2 P_{tx}(k)}{P_w(k)} \right) \quad [bps]. \tag{6}$$

We point out that the maximum achievable rate is a suitable metric to describe coverage.

E. Channel Delay

From the channel impulse response, we compute the delay that is introduced by the channel. We define it as the first time instant for which the absolute value of the impulse response exceeds the peak of the absolute value of the impulse response

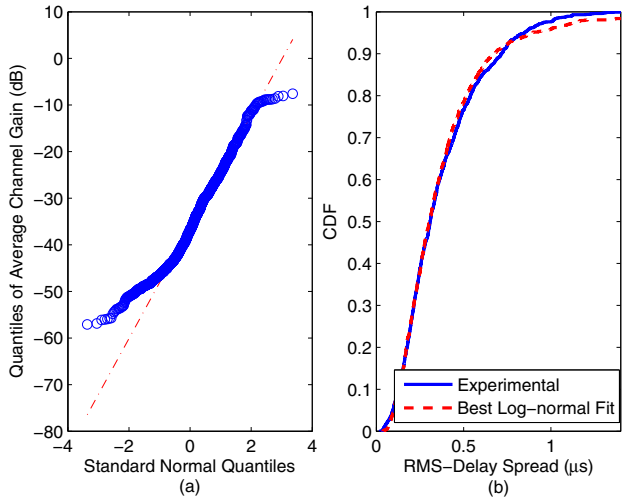

Fig. 2. On the left, quantiles of the average channel gain in dB versus the standard normal quantiles. On the right, cumulative distribution function of the RMS delay spread. The best log-normal fit is also shown.

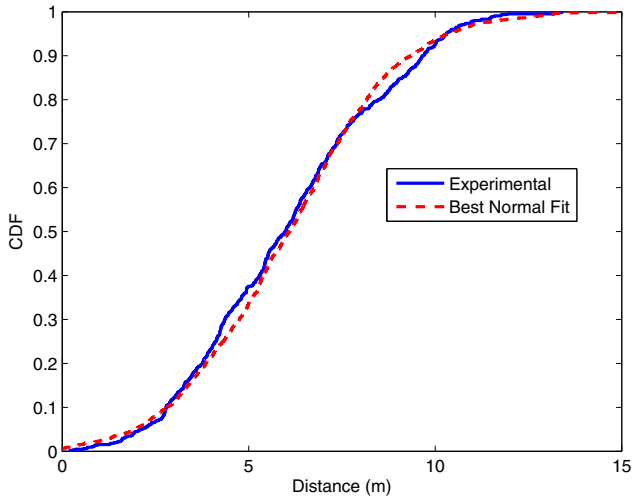

Fig. 3. Cumulative distribution function of the geometrical distance. The best fit is normal, and it is also shown.

by a constant factor α. Strictly, the channel delay is the time $T_d = \ell T$, where

$$\begin{aligned} \ell = & \underset{k=0,\ldots,2N-1}{\text{argmin}} \quad \{k\} \\ & \text{subject to } |h(k)| \geq \alpha \max\{|h(i)|\}, \\ & \qquad i = 0, \ldots, 2N-1, \\ & \qquad 0 < \alpha \leq 1. \end{aligned} \tag{7}$$

If $\alpha = 1$, the channel delay is the time instant that corresponds to the peak of the absolute value of the impulse response. In the following, we assume $\alpha = 1/2$. Finally, we note that the channel delay is related to the electrical distance. In fact, the channel delay is due to the propagation of the signal through the electrical wires. The longer the wires, the higher the delay.

IV. Numerical Results

We investigate the statistics of the measured channels and their dependence on the geometrical distance. To this aim, we merge the channels from all the measured topologies in a single set. Thus, we do not specialize the analysis to the individual topologies. Firstly, we focus on the distributions of the ACG and the RMS delay spread. The ACG in dB can be approximated as a normal random variable with mean -35.6 dB, and standard deviation 10.5 dB. The normality has been pointed out also in the literature. In Fig. 2a, we show the quantiles of the ACG versus the standard normal quantiles. Most of the samples lie on the dash-dotted line. It follows the normality. Slight deviations from normality are due to the fact that the the probability density function of the ACG exhibits a lower peak w.r.t. the one of the best normal fit. Strictly, the ACG is platykurtic because the kurtosis is 2.48.

The RMS delay spread is log-normally distributed. In Fig. 2b, we provide the cumulative distribution function (CDF) of the RMS delay spread of the measured channels. The best log-normal fit is also shown. As can be noted, the fit matches perfectly the experimental distribution. We point out that this result is consistent with the ones that have been previously reported in the literature [11].

In Fig. 3, we show the CDF of the distance between outlets in our measurement campaign. The distance ranges between 0.2 and 13.4 m. Furthermore, we note that the distance is normally distributed, with mean equal to 6 m, and standard deviation equal to 2.6 m. In this respect, we note that these values may vary from country to country due to the particular wiring structure, and the set of measured houses.

Now, we study the ACG as a function of distance. In Fig. 4a, we show the results. As expected, the ACG decreases with distance. We perform the robust regression fit of the measured data to obtain

$$G = -1.67d - 25.66 \quad [dB]. \tag{8}$$

We show the robust regression line in Fig. 4a. Furthermore, we note that the ACG is less spread as the channel length increases. In detail, the ACG of short channels, namely, below 5 m, varies from -50 dB to -10 dB. Conversely, when the distance is high, namely, more than 10 m, the ACG is concentrated in the range from -60 to -40 dB.

As for the ACG, we address the statistics of the RMS delay spread as a function of distance. We show the numerical results in Fig. 4b. From the robust regression fit, we note that the RMS delay spread increases with the distance as follows

$$\sigma_\tau = 0.023d + 0.196 \quad [\mu s]. \tag{9}$$

The maximum value of the RMS delay spread is approximately constant regardless distance. Conversely, we highlight the presence of a lower bound value. Basically, the minimum value of the RMS delay spread increases with distance.

Now, we study the maximum achievable rate as a function of distance. We show the results in Fig. 5a. The maximum

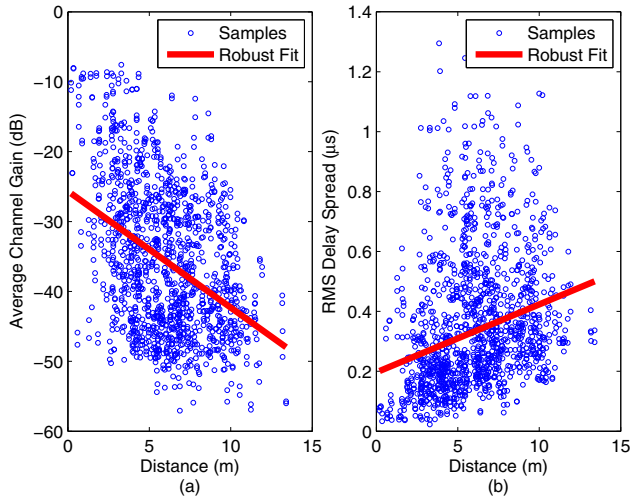

Fig. 4. On the left, average channel gain as a function of distance. On the right, RMS delay spread as a function of distance. In both cases, the linear robust fit is provided.

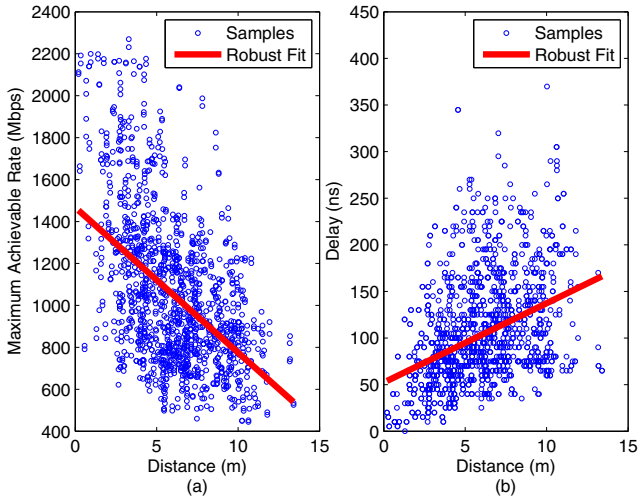

Fig. 5. On the left, maximum achievable rate as a function of distance. On the right, channel delay as a function of distance. In both cases, the linear robust fit is provided.

achievable rate is negatively related to the distance as follows

$$R = -69.3d + 1467.6 \quad [Mbps]. \tag{10}$$

Furthermore, we note that the maximum achievable rate of the channels with distance greater than 10 m is always lower than 1 Gbps, while the maximum value is 2.27 Gbps. From the maximum achievable rate, we infer coverage. We compute the complementary cumulative distribution function (C-CDF) of the maximum achievable rate of the channels whose length is smaller than 5 m, between 5 and 10 m, and greater than 10 m. We show the results in Fig. 6a. Channels that are shorter than 5 m exceed 1 Gbps in more than 70 % of the cases. In a dual manner, we study the CDF of the distance with achievable rate greater than 1.5, 1, and 0.5 Gbps. We show the results in Fig. 6b. Interestingly, the channels that exceed 1.5 Gbps are associated to outlets at distance that is smaller than 5 m in more than 80 % of the cases.

Finally, we address the channel delay as a function of distance. In Section III-E, we define the delay, and we set $\alpha = 1/2$. In Fig. 5b, we show the results. The PLC channel introduces a delay up to 425 ns. The delay is positively related to the distance. The robust fit of the data turns out the following relation

$$T_d = 8.51d + 52.22 \quad [ns]. \tag{11}$$

Interestingly, we note that the minimum value of the delay increases strictly with the channel length. Similar results can be obtained with smaller values of the constant coefficient α.

V. Channel Classification

We have shown that the statistics of the channel is a function of distance. Now, we classify channels according to the geometrical distance. For each class, we provide the mean value of the statistical metrics that we considered in Section III. Basically, the channel classification condenses the

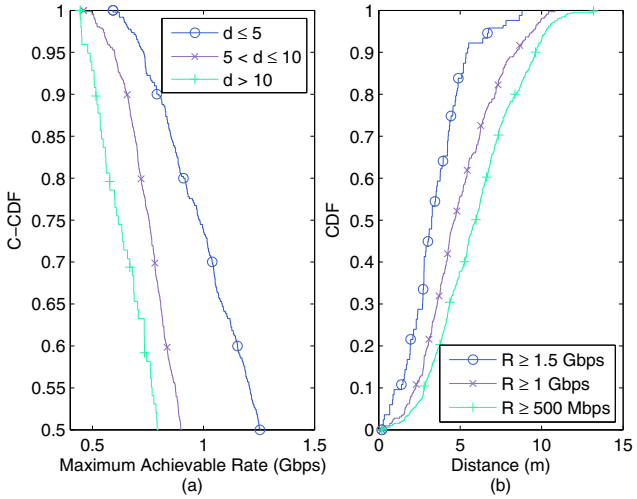

Fig. 6. On the left, complementary cumulative distribution function (C-CDF) of the maximum achievable rate for different ranges of distance. On the right, C-CDF of the distance for different values of achievable rate.

linear relations that we have presented in Section IV. Further, it provides a better understanding of coverage. We identify N_c classes as follows. We define the distance-step size Δ and we denote the class with the index c, where $c = 1, \ldots, N_c$. Class c collects all the channels whose length ranges between d_{min} and d_{max}, where

$$d_{min} = (c-1)\Delta, \tag{12}$$

$$d_{max} = \begin{cases} c\Delta & c < N_c \\ \infty & c = N_c. \end{cases} \tag{13}$$

In the following, we let N_c and Δ be equal to 5 and 2 m, respectively. In Table I, we report the values of d_{min} and d_{max} of each class.

We apply the channel classification to the measured data. We sort the measured channels into the 5 classes. In Table

I, we report the occurrence probability of each class, and we provide the mean value of the statistical metrics that we consider in Section III. We denote the mean value of the ACG, RMS delay spread, maximum achievable rate, and delay with $\overline{G}$, $\overline{\sigma}_\tau$, $\overline{R}$, and $\overline{T}_d$, respectively. Furthermore, in class 5, d_{max} is the length of the longest measured channel and, similarly, in class 1, d_{min} is the length of the shortest measured channel.

The classes show a remarkable distinct behaviour in terms of all the metrics. From class 1 to class 5, the mean value of the RMS delay spread doubles, and the variation of the channel delay is even higher. Finally, the maximum achievable rate ranges from 1.6 Gbps of class 1, to 865 Mbps of class 5, with an excursion of approximately 50 %.

VI. Conclusions

We have investigated the relation between the statistics of the PLC channel, and the geometrical distance between the transmitter and the receiver outlet. We have performed an experimental measurement campaign in Italy. We have collected channel frequency responses from different premises. In each premise, we have identified the representative outlets and we have measured the channel frequency response between all the couples of outlets. More than 1300 channels have been acquired.

Then, we have studied the statistics of the measured channels. We have found that the average channel gain in dB can be approximated with a normal random variable, while the RMS delay spread is log-normally distributed. These results are consistent with the ones that have been previously reported in the literature.

Finally, we have investigated the relation between the statistical metrics, and the geometrical distance. The analysis has been provided in terms of average channel gain, RMS delay spread, maximum achievable rate in the presence of stationary background noise, and channel delay. We have performed the robust fit of the measured data, and we have provided a linear relation between the metrics and distance. As expected, we have found that the average channel gain decreases with distance, while the RMS delay spread and the channel delay increase. Furthermore, the achievable rate decreases with distance, and thus, even in PLC, we can define coverage in terms of geometrical distance.

We have classified channels into 5 classes, according to the geometrical distance. For each class, we have provided the mean value of the metrics. In this respect, we have found that the classification according to the distance is valid because the mean value of the channel metrics shows a remarkable distinct behaviour for different classes.

TABLE I
Statistics of the classes

Metric		Class 1	2	3	4	5
occ. prob.	(%)	4.95	18.81	26.73	26.73	22.78
d_{min}	(m)	0	2	4	6	8
d_{max}	(m)	2	4	6	8	13.4
$\overline{G}$	(dB)	-23	-30	-36	-38	-40
$\overline{\sigma}_\tau$	(μs)	0.19	0.28	0.38	0.4	0.42
$\overline{R}$	$(Mbps)$	1617	1315	1084	963	865
$\overline{T}_d$	(ns)	44.8	82.0	107.6	117.6	135.2

References

[1] V. Oksman and S. Galli, "G.hn: The New ITU-T Home Networking Standard," *IEEE Commun. Mag.*, vol. 47, no. 10, pp. 138–145, Oct. 2009.

[2] S. Galli and O. Loginov, "Recent Developments in the Standardization of Power Line Communications within the IEEE," *IEEE Commun. Mag.*, vol. 46, no. 7, pp. 64–71, Jul. 2008.

[3] T. Esmailian, F. R. Kschischang, and P. Glenn Gulak, "In-Building Power Lines as High-Speed Communication Channels: Channel Characterization and a Test Channel Ensemble," *Intern. J. of Commun. Syst.*, vol. 16, no. 5, pp. 381–400, jun 2003.

[4] A. M. Tonello and F. Versolatto, "Bottom-Up Statistical PLC Channel Modeling - Part I: Random Topology Model and Efficient Transfer Function Computation," *IEEE Trans. Power Del.*, vol. 26, no. 2, pp. 891–898, Apr 2011.

[5] S. Galli and T. C. Banwell, "A Deterministic Frequency-Domain Model for the Indoor Power Line Transfer Function," *IEEE J. Sel. Areas Commun.*, vol. 24, no. 7, pp. 1304–1316, Jul. 2006.

[6] A. M. Tonello and T. Zheng, "Bottom-Up Transfer Function Generator for Broadband PLC Statistical Channel Modeling," in *Proc. IEEE Int. Symp. Power Line Commun. and its App. (ISPLC)*, Apr. 2009, pp. 7–12.

[7] S. Sancha, F. J. Canete, L. Díez, and J. T. Entrambasaguas, "A Channel Simulator for Indoor Power-Line Communications," in *Proc. IEEE Int. Symp. Power Line Commun. and its App. (ISPLC)*, Mar. 2007, pp. 104–109.

[8] A. M. Tonello and F. Versolatto, "Bottom-Up Statistical PLC Channel Modeling - Part II: Inferring the Statistics," *IEEE Trans. Power Del.*, vol. 25, no. 4, pp. 2356–2363, Oct. 2010.

[9] S. Galli and T. C. Banwell, "On the Symmetry of the Power Line," in *Proc. IEEE Int. Symp. Power Line Commun. and its App. (ISPLC)*, Apr. 2001, pp. 325–330.

[10] D. M. Pozar, *Microwave Engineering*. John Wiley & Sons, 2005.

[11] S. Galli, "A Simplified Model for the Indoor Power Line Channel," in *Proc. IEEE Int. Symp. Power Line Commun. and its App. (ISPLC)*, Apr. 2009, pp. 13–19.

[12] R. Hashmat, P. Pagani, and T. Chonavel, "MIMO Communications for Inhome PLC Networks: Measurements and Results up to 100 MHz," in *Proc. IEEE Int. Symp. Power Line Commun. and its App. (ISPLC)*, Apr. 2010, pp. 120–124.